NASA-TM-107031 19960013917

NASA Technical Memorandum 107031

Highlights of the Zeno Results From the USMP-2 Mission

Robert W. Gammon, J.N. Shaumeyer, Matthew E. Briggs,
Hacène Boukari, and David A. Gent
University of Maryland
College Park, Maryland

and

R. Allen Wilkinson
Lewis Research Center
Cleveland, Ohio

October 1995

National Aeronautics and
Space Administration

Highlights of the Zeno Results from the USMP-2 Mission

Robert W. Gammon, J. N. Shaumeyer, Matthew E. Briggs,
Hacène Boukari, and David A. Gent
Institute for Physical Science and Technology, University of Maryland, College Park, MD 20742

R. Allen Wilkinson
NASA/Lewis Research Center, Cleveland, OH 44135

I. INTRODUCTION

In a pure fluid near its liquid-vapor critical point, the otherwise small, statistical fluctuations in its density become as large as the wavelength of light when the system is still only 10 mK from the critical temperature, T_c. These large fluctuations scatter light very strongly, and the previously clear fluid turns milky white, a phenomenon known as critical opalesence.

Indeed, many different systems have critical points, and large fluctuations of some thermodynamic parameter are a universal feature. Because critical fluctuations become macroscopic and involve enormous numbers of molecules, many features of critical-point behavior are controlled by the statistical behavior of the fluctuations, so that many types of systems exhibit the same behavior near the critical point.

Light-scattering from critical fluctuations in a fluid is a simple and accurate technique to measure the decay rates of the fluctuations (the inverse of their lifetimes). However, near the critical point, the fluid becomes highly compressible, so the weight of the fluid alone causes severe density gradients in the sample, and distorts these measurements in a terrestrial laboratory.

The goal of the Zeno experiment was to build a precision, light-scattering spectrometer to measure the fundamental fluctuation decay rates in a sample of xenon. The spectrometer would operate in the low-gravity environment of the Space Shuttle, thus removing the gravity-induced distortion of the measurements. The instrument performed beautifully on its first mission and we were able to make our projected measurements with 1% precision to within 100 μK of the critical temperature (16.7 °C).

A schematic of the light-scattering spectrometer is shown in Fig. 1. Light from a low-power, helium-neon laser was directed into the sample along one of two beam paths determined by the beamsplitter (B 1): the path was chosen by shutters (S 1 and S 2). Light scattered by the sample (located in the cylindrical thermostat at the center of the figure) was then collected by the apertured photomultiplier tubes (PMT 1 and PMT 2), the primary signal that was processed to obtain the decay-rate information. In addition, photodiodes (PD 1 and PD 2) placed behind partially-reflecting mirrors (M 2 and M 3) measured the intensity of the light entering and exiting the sample. These two signals were then ratioed electronically to give us information about the turbidity of the fluid, which was an important measurement and our primary method of locating the critical temperature of the sample.

The collection angles for the scattered light (determined by apertures A1 through A4) were precisely aligned so the two scattering angles were supplementary. This simplified data analysis and allowed us to measure decay rates at the same pair of widely spaced angles, regardless of the beam path through the sample.

The instrument was housed in two separate containers attached to the USMP carrier. The optics module contained the light-scattering spectrometer, built on a stiff, optical bench, and temperature-sensitive signal amplifiers and ratio transformers for the thermostat's temperature control and measurement system. All additional electronics, including the instrument's computer system, were housed in the elecronics module.

II. TIMELINE

The instrument operated continuously for 13 days and 17 hours, which is probably a record. Figure 2 shows the timeline of the experiment as the temperature of the sample (in distance from T_c) versus MET. The principle events are delineated by times where the sample was warmed to $T_c + 1$K to bring it back to a state of uniform density, and times where the sample was closer than 1 μK to T_c.

During MET day 0 the instrument was primarily in a warm-up and initialization phase. Then, just prior to the start of MET day 1, the sample was warmed to 1 K, and the first scan to locate T_c began. The scan was followed by two warming periods. The slow cooling that spans MET days 2 and 3 represents a zig-zag search for T_c, which extended into MET day 4, followed by another warming procedure.

The first period of data collection began midway through MET day 4. Decay rate measurements were collected at a geometrically-spaced set of temperatures progressively nearer T_c, the first one starting at 100 mK. The last measurements of this set, during MET day 7, were within 100 μK of T_c, and actually contained some measurements at temperatures just below T_c.

MET day 8 began with another warming cycle, followed by another period of data collection at various temperatures between 560 mK and 30 μK above T_c. Between MET days 9 and 12, we took additional measurements at temperatures futher from T_c, and repeated selected measurements from earlier in the mission. Near the beginning of MET day 11 we began a series of 100-μK cooling steps that would again take the sample below T_c, recording decay rate measurements during the process with the hope of getting measurements that would show the effects of crossing the critical point into the two-phase region at temperatures at which it is impossible to make measurements on earth.

III. INSTRUMENT PERFORMANCE

A. Thermostat and Thermometry

The thermostat was a small device, 23-cm long and 8 cm in diameter, which provided a stable, controlled thermal environment for the xenon sample cell. It was made of three coaxial, cylindrical shells, each with a heater and feedback temperature controller. In addition, each shell and the sample cell had separate temperature-monitoring devices. Thermometry

was provided by thermistors inside the thermostat and sample-cell walls, wired to standard resistors inside the thermostat to form one arm of an AC-resistance bridge. The other part of the bridge was made of ratio transformers. In all there were three control bridges and one multiplexed measurement bridge. There were three six-decade ratio transformers and one eight-decade transformer, all calibrated through a collaboration with workers at the National Institute of Standards and Technology (see bibliography).

In flight, the thermostat required a stable thermal environment to do its job: the temperature control of the optics module by radiative heat leak and control heaters was excellent. Because of the mission length and the long periods of constant Shuttle attitude, we were able to maximize the temperature control. Thus, the thermostat was able to achieve a routine control level of better than ± 3-μK rms noise for periods of 3 hours or longer. Figure 3 shows one period of 4 hours when the sample cell temperature was controlled to 10-μK peak-to-peak (with a 5-second time constant in the measurement) and 1.7-μK rms. This level of control easily met the requirements for the Zeno experiment.

To change the temperature of the sample, the set points of all three control shells of the thermostat were moved. Figure 4 shows an example of a simple temperature change (cooling) of 2 mK; the temperature of the sample cell follows with a time constant of about 30 minutes.

For smaller temperature changes, we were able to make "fast steps" where the set points of the control shells were temporarily moved well beyond the target temperature and then returned just as the sample cell reached the desired temperature. Figure 5 illustrates the fast change, which is finished in a matter of minutes.

B. The Light-Scattering Spectrometer

Scattered light was detected by a pair of ruggidized, EMI 9863 photomultiplier tubes. These tubes had better than 5% quantum efficiency at 633 nm, total afterpulsing of less than 0.06%, and dark counts of less than 1 s^{-1} at the operating temperature of the optics module of 9°C. The background photon count rates were low enough that we could easily see the 20 counts/s from increased radiation when the Shuttle passed through the South Atlantic Anomaly.

The photomultiplier tubes were operated in photon-counting mode and the two signals were passed to the dual inputs of an ALV-5000 digital correlator, adapted specifically for this instrument. With this correlator, we were able to make simultaneous measurements of forward-scattered and backscattered light. The correlator is a special-purpose, digital signal processor, which produces an accurate autocorrelation function of the stream of photocounts from the photomultipliers. This correlator is designed to cover a broad range in delay times by calculating the autocorrelation function on a geometrically expanding time scale, so it is natural to plot the resulting correlograms with a logarithmic time scale. Figure 6 shows a sample correlogram; note that this shape represents an exponential decay of the autocorrelation function.

The experiment was performed with very low light levels. The windows of the sample cell absorb small amounts of the incident light at their surface (measured to be about 2 ppm). Because the thermal expansion coefficient of the sample diverges at the critical point, the increase in temperature of the window surface caused by absorbed light can

lead to unwelcome perturbations in the density of the fluid, and measurements would no longer represent the behavior of the fluid at the temperature we measured for the bulk (see bibliography).

To avoid these problems, we reduced the power of the laser light by placing filters in the beam paths, selecting two different power levels that allowed us to cover two temperature ranges with density perturbations of less than 1%. A power level of 17μW was used between 1 K and 1 mK from T_c, and the lower level of 1.7μW was used at temperatures closer than 1 mK, with overlapping measurements made with both powers near 1 mK. With this combination of incident light powers we were able to cover a wide range of temperature with enough signal to reach our precision requirement of 1% in the decay-rate measurements within the length of the mission.

IV. DETERMINING T_C ON ORBIT

Since all of the measurements in the Zeno experiment were made relative to the critical temperature of the xenon sample, it was important to understanding the results that we locate T_c precisely using our experimental thermometry. The possibility that the thermometry would be sensitive to the harsh mechanical environment of a Shuttle launch meant that locating T_c on orbit was a significant part of our mission activities.

In general, locating T_c involved moving the sample to a region very near the critical temperature and then adjusting its temperature in a controlled way and watching for signs that the critical point had been crossed. The signal that we monitored during the searches measured the turbidity of the sample, given by the logarithm of the ratio of the intensity of light transmitted by the sample to the intensity of the incident beam. We attempted two techniques with different expected levels of precision, only one of which worked.

The zig-zag technique, which we used to try to increase our level of precision for the value of T_c, didn't work successfully. This technique was used previously to locate the critical-mixing temperature of a density-matched mixture of two fluids. In a density-matched critical mixture, gravity has little effect and the technique gave clear indications, with 10-μK precision, whenever T_c was crossed. However, we could not try the technique with a pure-fluid system on Earth because the dynamics of density stratification were too rapid. Our single zig-zag search on orbit was the first time that this technique was tried in a pure fluid.

The zig-zag search started only 200μK above the critical temperature. Figure 7 shows how the temperature of the sample changed, alternately cooling by 20μK and then warming by 10μK. Figure 8 shows the response of the turbidity signal during the same portion of the search. Although it is clear that the sample is responding to the changes in temperature, we never detected a clear hysterisis in the turbidity that we expected that indicated we crossed T_c. We now believe that several unexpected effects in the turbidity signal (see section V) combined to obscure the transition. The entire period of the zig-zag search is shown in Fig. 9. At some point just past MET day 3, hour 12, the sample first crossed T_c and began the early stages of spinodal decomposition, indicated by the increasing amplitude of the variations in the signal. However, we will not be able to extract more precise information until we understand all of the effects in the turbidity response better.

Our second technique for locating T_c, which was successful, was a simple scanning procedure. The set point of the thermostat's control shells was changed in small steps of 50μK every 6 minutes (Fig. 10), which caused the temperature of the sample to change at a uniform rate of $500\,\mu$K/hour (Fig. 11).

During the scan, we monitored two signals as the sample crossed T_c: the turbidity of the sample, and the photon count rates of the light scattered by the sample. Figure 12 shows the turbidity signal during the first of the three scans done during the mission. Between hours 4 and 6, the signal increased steadily as the critical temperature was approached. At a few minutes past hour 6, there was a small break in the increase, followed by a swift rise and decline in the signal. The break marked the sample's crossing T_c; the large peak was caused by the sudden increase in density fluctuations as the fluid began spinodal decomposition, the initial stages of phase separation in which the fluctuations first become unstable and begin to grow. This increase passed as the fluid began to resolve itself into distinct gas and liquid phases, and the turbidity signal dropped.

The intensity of the forward-scattered light, shown over the same time period in Fig. 13, confirmed that this unassuming feature in the tubidity signal marked the phase boundary. The light scattered at this angle increased as the critical point was approached, and then dropped as fluctuations at this wavelength lost stability and the fluid began phase separation. The position of the peak in the scattering-intensity curve matched that of the feature in the turbidity curve.

For comparison, Fig. 14 shows a scan done on the instrument during preflight testing on the ground, at the same rate as the one in Fig. 12. There are two notable differences in the curves, both related to the effects of gravity. In the second hour of the terrestrial scan, the turbidity appeared to decrease rather than steadily increase. This was caused by the slowly forming density gradient in the highly compressible sample: as the gradient became more severe, the amount of fluid near enough to its critical density to show increasing turbidity decreased, and the net effect was a decrease in the turbidity signal. In addition, the small feature immediately preceeding the phase-decomposition peak that marked the phase transition is not visible. At this level of resolution, gravity broadened the critical point to such an extent that it effectively disappeared from the turbidity response.

During the mission, the collection of three scans and the zig-zag T_c determinations seemed to show a drift in the critical temperature of 800μK, substantially larger than what was seen during all testing with this instrument and with the functionally identical engineering model. However, we now believe that this may have been caused by small density rarifications in the beam path that resulted from repeated crossings into the two-phase region that were not completely removed by the warming procedures that we used to rehomogenize the sample. Subsequent ground scans with the instrument, along with the first on-orbit scan and previous ground measurements now tell us unambiguously that the critical temperature of the sample was stable during the mission to within the ± 50-μK precision of our measurement. This gives an upper bound of $120\,\mu$K/year on the stability of this sample: a drift rate spectacularly better than any previously experienced.

V. TURBIDITY MEASUREMENTS AND RELATED EFFECTS

Turbidity is the natural logarithm of the sample transmission per unit length, and is a measure of the overall cloudiness of the sample. We measured the intensity of the light leaving the sample and ratioed that with the intensity of the light entering the sample. Special electronics then calculated the logarithm of this ratio, giving us a measurement proportional to the turbidity of the xenon sample.

The turbidity of a fluid increases as the fluid is taken nearer to its critical point and measuring the turbidity gives information about the average size (correlation length) of critical fluctuations. The turbidity measurements that we made during the mission proved to be the biggest challenge to our understanding the flight data. During the mission, the turbidity signal showed small, long-time drifts at constant temperatures, sometimes to smaller values, sometimes to larger values. We believe that this was related to the small density inhomogeneities that we conjecture caused the apparent drifts in T_c. However, the analysis of these data are far from complete at this point.

Extracting values that actually represent the turbidity of the sample is complicated by two known effects that make difficult a direct, simple turbidity measurement. We have modeled these effects extensively and now have a better understanding of their contribution. The first has to do with the optical properties of the sample cell itself, and the second is a manifestation of the thermal response of a fluid near its critical point.

The interior of the sample cell created a 100-μm-thick disk of xenon, which was the portion of the sample that the laser beam passed through, by bounding the region with two polished, parallel, fused-quartz windows. Reflections of the beam from the window surfaces can interfere, changing the intensity of the transmitted beam depending on the spacing of the windows. When the temperature of the sample cell was changed, thermal expansion or contraction of its components altered the window spacing and produced a measurable change in the turbidity signal, independent of the xenon's turbidity.

Figure 15 shows the turbidity signal responding to 100-mK steps in the temperature of the sample cell, which warmed the cell from 1 to 5 K above the critical temperature of the xenon. This curve is from preflight testing of the instrument. At these temperatures, the actual turbidity of the fluid is negligible and we are viewing the interferometric behavior of the sample cell only.

The large, sinusoidal variations in the curve were the result of the interference effect, showing that the separation of the windows changed by about 0.75 orders of interference per Kelvin, at approximately 400 orders of interference. This corresponded to a rather small change in the window separation of 0.28 μm/K. Nevertheless, it is clear from the magnitude of the change in Fig. 15, that in order to make good use of our turbidity measurements, it is vital that we know where the measurements were made on this interference curve.

We fit curves like this one with ample precision to make the necessary correction to the turbidity measurements. Important questions about how this characteristic of the instrument changes with time are now settled. From analysis of testing before and after the mission, we found that the amplitude of this curve was stable and predictable. However, the phase of the interference showed a drift with time, which suggests that the sample cell exhibits a small mechanical creep of its longitudinal spacing of about 10 nm/month. With this information, we can be confident that we placed the flight measurements at the appropriate

place on the interference curve.

There is a second feature evident in Fig. 15 that is related to the fluid behavior itself. With each temperature step, the turbidity signal overshot and then returned to the expected value rather than simply moving to a new value appropriate to that temperature. All of these temperature steps were of the fast-change variety. Although the fluid at these temperatures showed no critical enhancement to its turbidity, it was still near enough to the critical point that it was highly compressible. In previous work (see bibliography), we have shown that highly-compressible critical fluids can make very fast changes in their density via an adiabatic heat-transfer mechanism; this phenomenon is a manifestation of the adiabatic mechanism.

As the temperature change began, heat entered the outer walls of the sample cell and quickly caused a large thermal expansion of a thin layer (order 10 μm) of fluid near the wall. Because of high compressibility, the bulk of the fluid was subject to adiabatic compression, which caused the bulk to heat rapidly. Significantly, the density of the bulk changed, which changed its index of refraction, hence the optical path length of the laser beam that passed through that part of the sample. Thus, during the temperature change, the fluid in the optical path of the cell executed density changes that affected the interference characteristics of the cell. Note that this transient response depends on the temperature of the fluid and decreased as the sample was moved further from T_c.

We have been modeling this phenomenon extensively, and performing controlled experiments with our engineering model of the instrument. These analyses have now converged in a satisfying way.

Figure 16 demonstrates the adiabatic effect, using data from the engineering model. The sample cell was subjected to a fast change of 100 mK, far enough from T_c that the actual turbidity of the xenon is negligible. Recorded in the lower curve is the response in the measured turbidity signal showing the overshoot and then return to its final, equilibrium value. It is significant that the final value is reached at precisely the same time as the temperature change is completed.

From our calibration of the apparent change in turbidity, the upper curve in Fig. 16 shows data represented as a change in phase along the interference curve, caused solely by the interference effects of cell expansion. The difference between these two curves, shown in Fig. 17, shows the effect resulting solely from a change in the fluid density from adiabatic heating effects. Since the adiabatic effects came into play only in response to a changing temeprature, we can verify this relationship by comparing the adiabatic response in Fig. 17 to Fig. 18, which is the derivative of the sample-cell temperature measured during the temperature change; they have exactly the same shape. Note that the temperature is measured at the cell wall, approximately 1.5 cm from the region of fluid probed by the laser, confirming the long-range action of the adiabatic effect.

All of the mysteries of the flight turbidity data are not settled. Figure 19 shows the transient response of the turbidity signal when the sample cell temperature was changed by 70 mK (starting from $T_c + 0.1\,\mathrm{K}$). The adiabatic contribution that we have measured on Earth is evident here in the initial sudden decrease in the signal as the temperature change began. However, this was soon overwhelmed by a much larger change in the opposite direction, followed by a slower settling to the final value. We know that this response is apparent because gravity was removed: we never saw it in data taken during ground testing. We believe that it is related to later stages in an adiabatic response that is quenched by

convection in 1 g, but we have not yet completed the modeling of the behavior.

VI. CRITICAL-POINT FLUCTUATION DECAY RATES

During the mission, we collected 32 sets of correlograms at 23 different temperature set-points, covering a temperature range from 560 mK to 10 μK above the critical temperature, as well as three temperatures below critical. In all, there are 500 correlograms for each of the two scattering angles (in the fluid) of 10.4478° (forward scattering) and 169.5636° (backscattering); forward scattering and backscattering correlograms were collected simultaneously. The data were taken with two different incident-beam intensities: 17 and 1.7 μW.

The next several figures show representative correlograms, illustrating the range of temperatures and incident-beam intensities. Figure 20 shows a pair of correlograms taken 560 mK from T_c, the furthest from the critical temperature at which we made measurements. As in all the correlograms, the upper curve with the slower decay is the forward-scattering correlogram. At this temperature, the intensity of the scattered light was at its lowest, although we used the higher power beam path. Although the measurements are statistically meaningful, the decays of the two curves, particularly the backscattering curve, are barely discernable.

Figure 21 shows a pair taken 1 mK above the critical temperature, using the higher-intensity beam path. At this temperature, the critical fluctuations were well developed, the intensity of the scattered light was relatively high in both directions, and the correlograms appeared virtually noiseless. However the backscattering correlogram shows two decays, which is a new feature. The second decay has the same time scale as the forward-scattering correlogram and is actually forward scattered light.

The forward-scattering cross section became large enough, 100 times the backscattering cross section, that the small amount of light reflected in the backward direction at the exit window of the sample cell contributed a forward-scattering correlation to this signal. It was for this reason that the two scattering angles were chosen to be precise supplements. Results from the analysis of the forward-scattering correlograms could be used to remove this contribution from the backscattering correlograms.

For comparison, Fig. 22 shows a pair of correlograms at the same temperature as in Fig. 21, but at the lower beam intensity of 1.7 μW. The backscattering correlogram shows an increased amount of noise (caused by the statistical process of the light detection), but the decay rate obtained from it is still precisely determined. Finally, Fig. 23 shows correlograms collected at T_c+100 μK. These measurements are well inside a region in which the observation of fluctuation correlations on Earth is completely distorted by gravity.

The data sets were collected for a total amount of time that we had predicted would result in fluctuation decay-rate measurements with a precision of 1% or better. We achieved this precision with all of the measurements except for the backscattering measurement at the warmest temperature, where the extremely low intensity of the scattered light precluded it. Each data set was made up of 10 to 15 separate correlograms so we could examine our results statistically.

The decay-rate values were extracted from the correlograms by nonlinear, least-squares fitting. The forward-scattering correlograms were fit to a simple decaying exponential; for

the backscattering correlograms the forward-scattering contribution was first removed where necessary, and then a simple decaying exponential was used.

The results of the fluctuation decay-rate measurements are shown in Fig. 24, the backscattering decay rates, and Fig. 25, the forward-scattering decay rates. We included data from ground testing on the instrument in both figures (in both cases the upper curve of symbols), and a line representing the best available theoretical predictions.

Quite evident in these graphs is the effect of removing gravity and the distortions it creates in the density of the sample, which are already apparent as far as 30 mK from the critical temperature. The limiting values of these curves is a significant measurement, and it is clear from these graphs that it is not possible to make accurate measurements of the limits on Earth, whereas we penetrated well into the limiting region without the distortions resulting from gravity. As measurements were made closer to T_c, the density gradient in the Earth-bound sample as probed by the 100-μm diameter of our focused laser beam, errors of 100% occurred, doubling the apparent decay rate in the terrestrial measurements compared with the measurements in μg.

We believe that the limiting values of the fluctuation decay rates from our data set will be the key contributions from this flight of the Zeno instrument. Some questions remain about the homogeneity and precise density of the xenon at each temperature because of the drifts in the turbidity signal. Nevertheless, we made measurements so close to the critical temperature that we made accurate measurements of the limiting values of the decay rate, regardless of the possibly small variations in density. These limits are beyond the predictive capabilities of current theories and represent a challenge and target for future calculations of transport properties in near-critical systems.

To conclude, we present our results for the limits. From the backscattering, the limiting decay rate is $\Gamma = (51.2 \pm 0.4) \times 10^3\,\mathrm{rad/s}$ at a scattering angle in the fluid of 169.5636°. From the forward scattering, the limiting decay rate is $\Gamma = 36.8 \pm 0.3\,\mathrm{rad/s}$ at a scattering angle inside the fluid of 10.4478°.

VII. CONCLUSION

The Zeno instrument and the special flight opportunity of the USMP-2 mission, with its exceptional commitment of mission time to making fundamental scientific measurements, gave us an excellent data set to contribute to measurements on liquid-vapor critical points. The data are beautiful and precise. The outstanding performance of the Zeno instrument during the mission gave a fine demonstration of the possibility of making high-precision, materials measurements in low gravity, as well as the power of a flexible, ground-commanded experiment.

VIII. ACKNOWLEDGEMENTS

We are grateful for the work of many colleagues who contributed so much to the success of this mission. At the University of Maryland: John Borden, David Torrealba, Dan Swann, Mark Sienkiewicz, Paul Mahata, Lori Mora, Matt Bieneman, Meade Larson, John

Pickett, Kai-Chang Zhang, Ed Cole, and Jan Sengers. At the NASA Lewis Research Center: Richard Lauver, Andrew Peddie, Greg Zimmerli, Geoff Elliott, and Klaus Gumpto. At Ball Aerospace: Richard Reinker, Mike Dials, Robert Stack, and Robert Woodruff. At the National Institute of Standards and Technology: Svetlana Avramov, Nile Oldham, M. R. Moldover, and Robert Berg.

IX. SELECTED BIBLIOGRAPHY

A. Zeno Publications

Robert W. Gammon and J.N. Shaumeyer, "Science Requirements Document for Zeno" (NASA, Washington D.C., 1988).

Ronald B. Kopelman, "Light Scattering Measurements of Critical Fluctuations in an Optically Thin Binary Liquid Sample," Ph.D. dissertation, University of Maryland, College Park, MD, 1983 (University Microfilms, Ann Arbor, #AAD84-05662).

M. R. Moldover and R. W. Gammon, "Capillary Rise, Wetting Layers, and Critical Phenomena in Confined Geometry," J. Chem. Phys. **80**, 1984, pp. 528–535.

R. K. Kopelman, R. W. Gammon, and M. R. Moldover, "Turbidity Very Near the Critical Point of Methanol-Cyclohexane Mixtures," Phys. Rev. **A29**, 1984, p. 2084.

Yasunari Takagi and Robert W. Gammon, "Brillouin-Scattering in Thin Samples: Observation of Backscattering Components by 90° Scattering," J. Appl. Phys. **61**, 1987, pp. 2030–2034.

R. W. Gammon, "Critical Fluid Light Scattering," in *The Nation's Future Material Needs*, T. Lynch, J. Persh, T. Wolf, and N. Rupert, eds. (Soc. Adv. Mater. & Process Eng., Covina, CA, 1987), proceedings of the 19th International Technical Conference of the Society for the Advancement of Material and Process Engineering (SAMPE), Oct. 13–15, 1987.

J. N. Shaumeyer and Robert W. Gammon, "Optimizing Fitting Statistics in Photon Correlation Spectroscopy," in *OSA Proceedings on Photon Correlation Techniques and Applications, Volume I*, John B. Abbiss and Anthony E. Smart, eds. (Optical Society of America, Washington, D.C., 1988), pp. 14–17.

R. W. Gammon, "Description of the Photon-Correlation Instrument for Zeno," NASA Laser Light Scattering Advanced Technology Development Workshop, NASA Lewis Research Center, Sept. 1988. NASA Conference Publication 10033 (1989).

Hacène Boukari, J. N. Shaumeyer, Matthew E. Briggs, and Robert W. Gammon, "Critical Speeding Up in Pure Fluids," Phys. Rev. A **41**, 1990, pp. 2260–2263.

Hacène Boukari, Matthew E. Briggs, J. N. Shaumeyer, and Robert W. Gammon, "Critical Speeding Up Observed," Phys. Rev. Lett. **65**, 1990, pp. 2654–2657.

R. W. Gammon, "Investigations of Fundamental Phenomena in Microgravity," Proceedings IKI/AIAA Microgravity Symposium (American Institute of Aeronautics and Astronautics, 1991), pp. 379–381.

J. N. Shaumeyer, Robert W. Gammon, and J. V. Sengers, "Photon-Correlation Spectroscopy," in *Measurement of the Transport Properties of Fluids, Experimental Thermodynamics, Volume III*, W.A. Wakeham, A. Nagashima, and J.V. Sengers, eds. (Blackwell Scientific, Oxford, 1991), pp. 197–213.

Hacène Boukari, "Adiabatic Effects in a Fluid near its Liquid-Gas Critical Point: Theory and Experiment," Ph.D. dissertation, University of Maryland, College Park, MD, 1992.

K. C. Zhang, M. E. Briggs, and R. W. Gammon, "The Susceptibility Critical Exponent for a Nonaqueous Ionic Binary Mixture near a Consolute Point," J. Chem. Phys. **97**, 1992, pp. 8692–8697.

Matthew E. Briggs, "Photothermal Deflection in a Supercritical Fluid," Ph.D. dissertation, University of Maryland, College Park, MD, 1993.

Matthew E. Briggs, Robert W. Gammon, and J. N. Shaumeyer, "Measurement of the Temperature Coefficient of Ratio Transformers," Rev. Sci. Instrum. **64**, 1993, pp. 756–759.

S. Avramov and N. M. Oldham, "Automatic Calibration of inductive Voltage Dividers for the NASA Zeno Experiment," Rev. Sci. Instrum. **64**, 1993, pp. 2676–2678.

S. Avramov and N. M. Oldham, "Inductive Voltage Divider Calibration for a NASA Flight Experiment," National Conference of Standards Laboratories Workshop and Symposium (Albuquerque, NM, July 1993) Proceedings, 1993, pp. 225–232.

J. N. Shaumeyer, Matthew E. Briggs, and Robert W. Gammon, "Statistical Fitting Accuracy in Photon Correlation Spectroscopy," Appl. Optics **32**, 1993, pp. 3871–3879.

Svetlana Avramov, "Voltage Ratio Measurements using Inductive Voltage Dividers," Ph.D. dissertation, University of Maryland, College Park, MD, 1994.

E. D. Palik, Hacène Boukari, and Robert W. Gammon, "Line-Shape Studies for Single- and Triple-Pass Fabry-Perot Interferometer Systems," Appl. Optics **34**, 1995, pp. 58–68.

Hacène Boukari, E. D. Palik, and R. W. Gammon, "Closed-Form Expressions to Fit Data Obtained with a Multipass Fabry-Perot Interferometer System," Appl. Optics **34**, 1995, pp. 69–86.

Hacène Boukari, Robert L. Pego, and Robert W. Gammon, "Calculation of the Dynamics of Gravity-Induced Density Profiles near a Liquid-Vapor Critical Point", Phys. Rev. E **52**, 1995, pp. 1614–1626.

B. NASA Reports

R. W. Gammon and M. R. Moldover, "Light Scattering Tests of Fundamental Theories of Transport Properties," in *Microgravity Science and Applications Program Tasks*, NASA Technical Memorandum 89607 (NASA Office of Space Science and Applications, Washington, D.C., February 1985), p. 240.

R. W. Gammon and M. R. Moldover, "Light Scattering Tests of Fundamental Theories of Transport Properties," in *Microgravity Science and Applications Program Tasks*, NASA Technical Memorandum 87568 (NASA Office of Space Science and Applications, Washington, D.C., May 1986), p. 106.

Robert W. Gammon, "Critical Fluid Light Scattering," in *Microgravity Science and Applications Flight Programs, January–March 1987, Selected Papers*, NASA Technical Memorandum 4069, Vol. 2 (NASA Office of Space Science and Applications, Washington, D.C., 1988), p. 805.

R. W. Gammon, J. N. Shaumeyer, and M. R. Moldover, "Zeno: Critical Fluid Light Scattering," in *Microgravity Science and Applications Program Tasks: 1987 Revision*, NASA Technical Memorandum 4068 (NASA Office of Space Science and Applications, Washington, D.C., September 1988), p. 189.

R. W. Gammon, J. N. Shaumeyer, and M. R. Moldover, "Zeno: Critical Fluid Light Scattering," in *Microgravity Science and Applications Program Tasks: 1988 Revision*, NASA Technical Memorandum 4097 (NASA Office of Space Science and Applications, Washington, D.C., January 1989), p. 245.

R. W. Gammon, and J. N. Shaumeyer, "Critical Fluid Light Scattering (Zeno)," in *Microgravity Science and Applications Program Tasks: 1989 Revision*, NASA Technical Memorandum 4191 (NASA Office of Space Science and Applications, Washington, D.C., May 1990), p. 201.

R. W. Gammon, and J. N. Shaumeyer, "Critical Fluid Light Scattering (Zeno)," in *Microgravity Science and Applications Program Tasks: 1990 Revision*, NASA Technical Memorandum 4284 (NASA Office of Space Science and Applications, Washington, D.C., May 1991), p. 261.

R. W. Gammon, and J. N. Shaumeyer, "Critical Fluid Light Scattering (Zeno)," in *Microgravity Science and Applications Program Tasks: 1991 Revision*, NASA Technical Memorandum 4349 (NASA Office of Space Science and Applications, Washington, D.C., February 1992), p. 261.

R. W. Gammon, "Critical Fluid Light Scattering (Zeno)," in *Microgravity Science and Applications Program Tasks and Bibliography for FY 1992*, NASA Technical Memorandum 4469 (NASA Office of Space Science and Applications, Washington, D.C., March 1993), p. II-69.

C. Critical Phenomena

1. Static Critical Phenomena

Albert Einstein, Ann. Phys. (Leipzig) **33**, 1275 (1910); english translation: "Theory of Opalescence of Homogeneous Liquids and Mixtures of Liquids in the Vicinity of the Critical State," in *Colloid Chemistry*, J. Alexander, ed. (Rheinhold, New York, 1913), Vol. I, p. 323.

H. Eugene Stanley, *Introduction to Phase Transitions and Critical Phenomena* (Oxford, New York, 1971).

Kenneth G. Wilson and J. Kogut, "The Renormalization Group and the ϵ Expansion," Phys. Rep. **12C**, 1974, p. 77.

2. Dynamic Critical Phenomena

Harry L. Swinney and Donald L. Henry, "Dynamics of Fluids near the Critical Point: Decay Rate of Order-Parameter Fluctuations," Phys. Rev. **A8**, 1973, p. 2586.

K. Kawasaki, in *Phase Transitions and Critical Phenomena*, C. Domb and M.S. Green, eds. (Academic, New York, 1975), Vol. 5a, p. 165.

E. D. Siggia, B. I. Halperin, and P. C. Hohenberg, "Renormalization-Group Treatment of the Critical Dynamics of the Binary-Fluid and Gas-Liquid Transitions," Phys. Rev. **B13**, 1976, p. 2110.

Hannes Güttinger and David S. Cannell, "Correlation Range and Rayleigh Linewidth of Xenon near the Critical Point," Phys. Rev. **A22**, 1980, p. 285.

J. V. Sengers, "Universality of Critical Phenomena in Classical Fluids," in *Phase Transitions: Cargese 1980*, Maurice Levy, Jean-Claude LeGuillou, and Jean Zinn-Justin, eds. (Plenum Publishing Corp., New York, 1982).

Jayanta K. Bhattacharjee and Richard A. Ferrell, "Critical Viscosity Exponent for a Classical Fluid," Phys. Rev. **A28**, 1983, p. 2363.

H. C. Burstyn, J. V. Sengers, J. K. Bhattacharjee, and R. A. Ferrell, "Dynamic Scaling Function for Critical Fluctuations in Classical Fluids," Phys. Rev. **A28**, 1983, p. 1567.

R. F. Berg and M. R. Moldover, "Critical Exponent for the Viscosity of Carbon-Dioxide and Xenon," J. Chem. Phys. **93**, 1990, p. 1926.

Hong Hao, "Aspects of Dynamic Critical Phenomena in a Single-Component Fluid," Ph.D. dissertation, University of Maryland, College Park, MD, 1991.

D. Critical-Fluid Light Scattering

V. G. Puglielli and N. C. Ford, Jr., "Turbidity Measurements in SF_6 near its Critical Point," Phys. Rev. Lett. **25**, 1970, p. 143.

V. Degiorgio and J. B. Lastovka, "Intensity-Correlation Spectroscopy," Phys. Rev. **A4**, 1971, p. 2033.

Joseph H. Lunacek and David S. Cannell, "Long-Range Correlation Length and Isothermal Compressibility of Carbon Dioxide Near the Critical Point," Phys. Rev. Lett. **27**, 1971, p. 841.

N. C. Ford, Jr., "Light Scattering Apparatus", in *Dynamical Light Scattering, Application of Photon Correlation Spectroscopy*, R. Pecora, ed. (Plenum, New York, 1985), p. 7.

E. Low-Gravity Critical Phenomena

P. C. Hohenberg and M. Barmatz, "Gravity Effects near the Gas-Liquid Critical Point," Phys. Rev. **A6**, 1977, p. 289.

M. R. Moldover, R. J. Hocken, R. W. Gammon, and J. V. Sengers, *Overviews and Justifications for Low Gravity Experiments on Phase Transitions and Critical Phenomena in Fluids*, National Bureau of Standards Technical Note 925 (U.S. Government Printing Office, Washington, D.C., 1976).

M. R. Moldover, J. V. Sengers, R. W. Gammon, and R. J. Hocken, "Gravity Effects in Fluids near the Gas-Liquid Critical Point," Rev. Mod. Phys. **51**, 1979, p. 79.

D. Beysens, "Critical Phenomena," in *Materials Sciences in Space, a Contribution to the Scientific Basis of Space Processing*, B. Feuerbacher, H. Hamacher, and R.J. Naumann, eds. (Springer, Berlin, 1986), p. 191.

D. Beysens, J. Straub, and D. J. Turner, "Phase Transitions and Near-Critical Phenomena," in *Fluid Sciences and Materials Science in Space, A European Perspective*, H. U. Walter, ed. (Springer, Berlin, 1987), p. 221.

D. Beysens, "Recent Developments in Critical and Near-Critical Point Phenomena," in *Proceedings VIIth European Symposium on Materials and Fluid Sciences in Microgravity*, ESA **SP-295**, 1990.

P. Guenoun, B. Khalil, D. Beysens, Y. Garrabos, F. Kammoun, B. Le Neindre, and B. Zappoli, "Thermal Cycle Around the Critical-Point of Carbon-Dioxide under Reduced Gravity," Phys. Rev. **E47**, 1993, p. 1531.

F. Adiabatic Effects near the Critical Point

D. Dahl and M. R. Moldover, "Thermal Relaxation Near the Critical Point," Phys. Rev. **A6**, 1972, p. 1915.

A. Onuki, H. Hong, and R. A. Ferrell, "Fast Equilibration in a Single-Component Fluid Near the Liquid-Vapor Critical Point," Phys. Rev. **A41**, 1990, p. 2256.

A. Onuki and R. A. Ferrell, "Adiabatic Heating Effect Near the Gas-Liquid Critical Point," Physica **A164**, 1990, p. 245.

R. P. Behringer, A. Onuki, and H. Meyer, "Thermal Equilibration of Fluids Near the Liquid-Vapor Critical-Point–^{3}He and ^{4}He Mixtures," J. Low Temp. Phys. **81**, 1990, p. 71.

B. Zappoli, D. Baily, Y. Garrabos, B. Le Neindre, P. Guenoun, and D. Beysens, "Anomalous Heat Transport by the Piston Effect in Supercritical Fluids under Zero Gravity," Phys. Rev. **A41**, 1991, p. 2264.

R. A. Ferrell and H. Hao, "Adiabatic Temperature Changes in a One-Component Fluid Near the Liquid-Vapor Critical Point," Physica **A197**, 1993, p. 23.

R. F. Berg, "Thermal Equilibration Near the Critical Point: Effects due to Three Dimensions and Gravity," Phys. Rev. **E48**, 1993, p. 1799.

F. Zhong and H. Meyer, "Numerical Calculation of Density Equilibration Above the ^{3}He Liquid-Vapor Critical Point," in *Proceedings of NASA/JPL Microgravity Low Temperature Workshop, Washington, D.C (1994)*, U. Israelson and D. Strayer, eds., NASA Document JPL D-11775 (NASA, Washington D.C., 1994), p. 73.

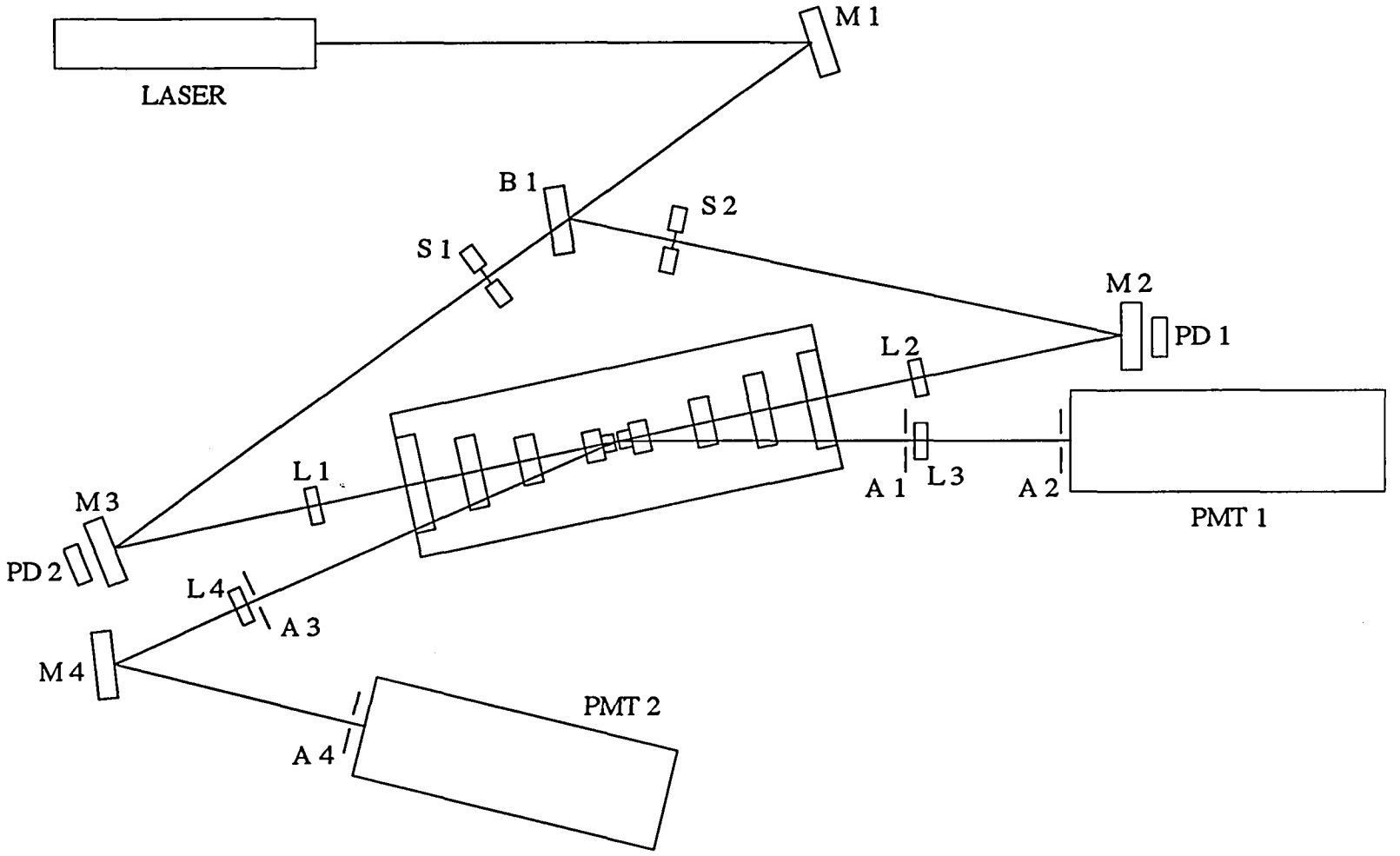

FIG. 1 Optical layout of the instrument, showing main components: beamsplitter (B 1), mirrors (M 1, M 2, and M 3), apertures (A 1 through A 4), photodiodes (PD 1 and PD 2), shutters (S 1 and S 2), and photomultiplier tubes (PMT 1 and PMT 2). The thermostat is the cylindrical object in the center.

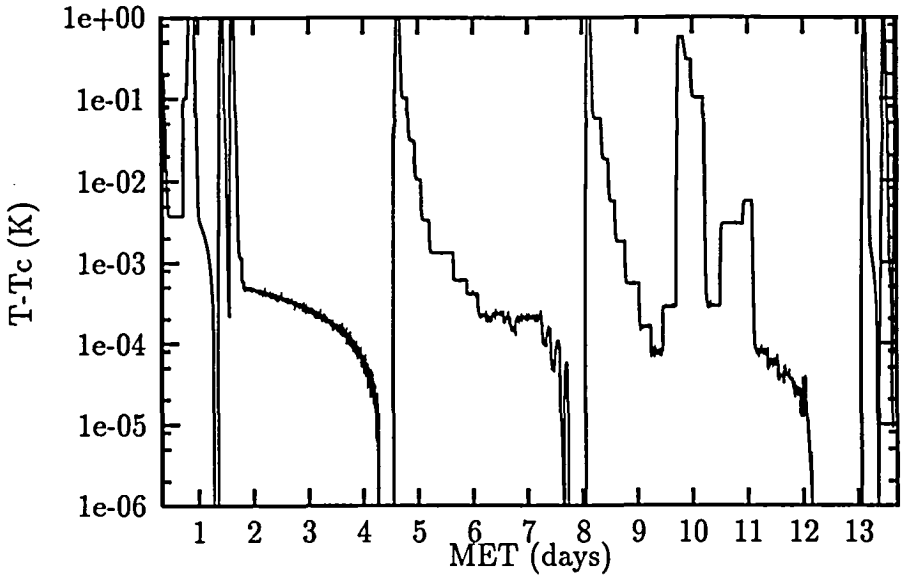

FIG. 2 The experiment timeline, given as the temperature of the sample (measured in distance from T_c) versus mission elapsed time in days.

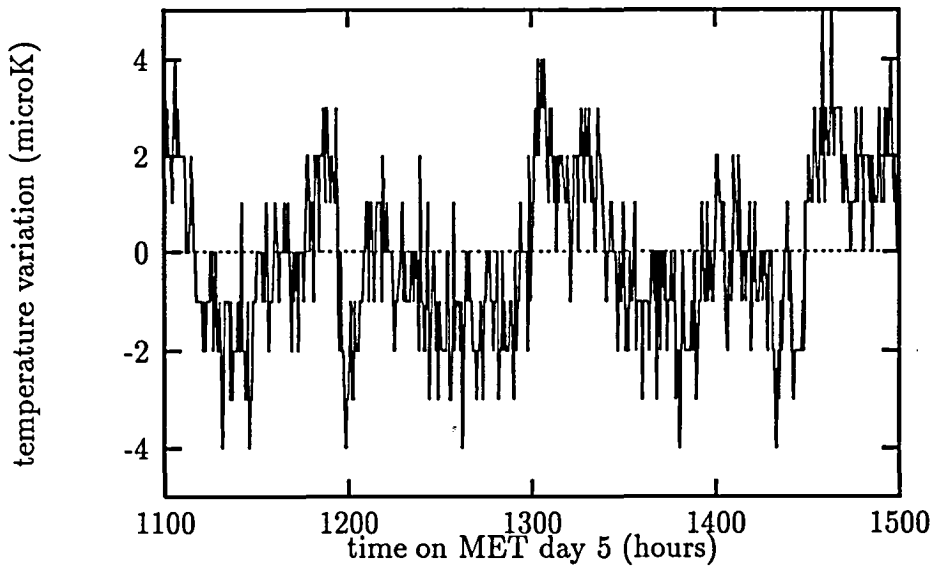

FIG. 3 Stability of the sample temperature at 1 mK, over a 4-hour period while collecting correlograms. The rms of the variations is 1.7 μK. (Time is in *hhmm* format.)

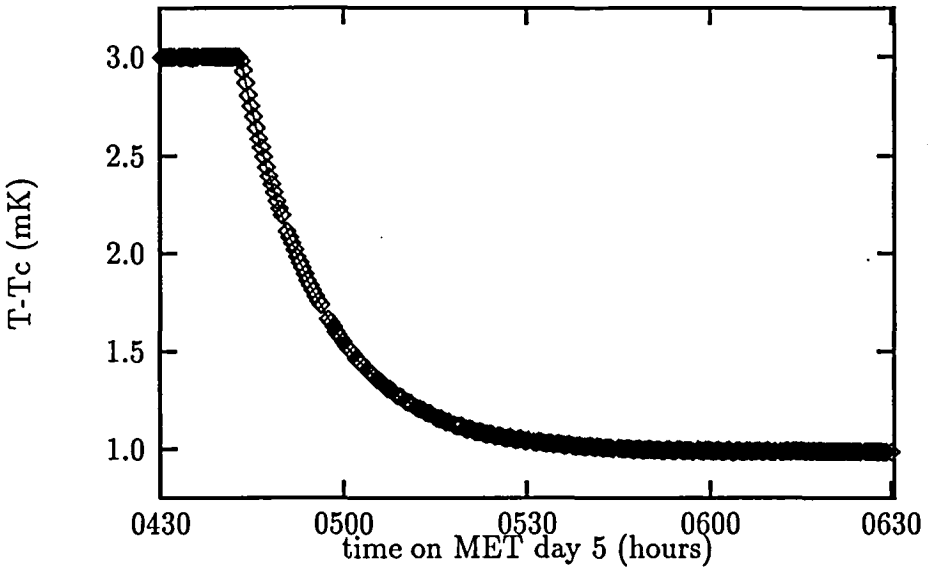

FIG. 4 The temperature of the sample cell during a slow temperature step of -2 mK, shown as distance from T_c. The time constant for thermal relaxation of the sample cell is about 30 minutes. (Time is in *hhmm* format.)

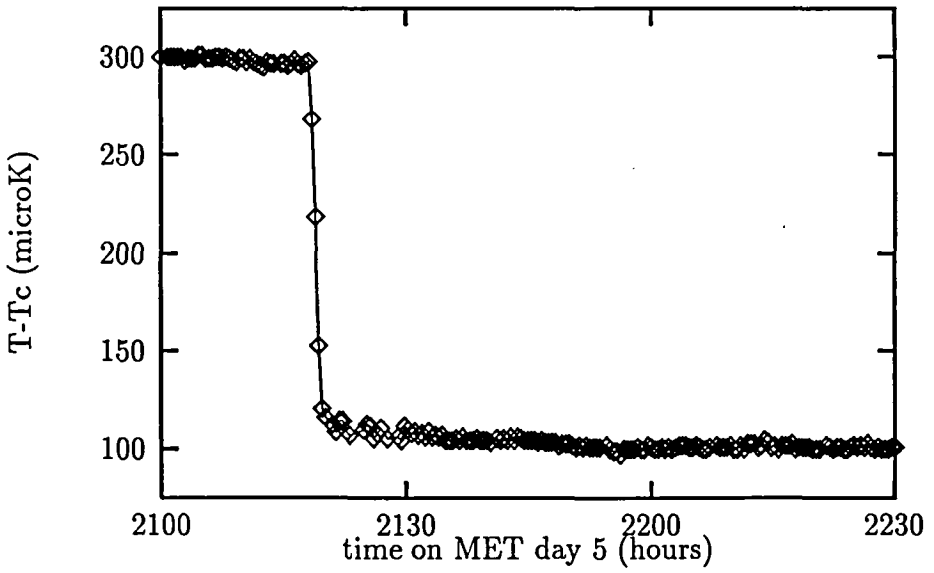

FIG. 5 The temperature of the sample cell during a fast temperature step of $-200\,\mu$K, shown as distance from T_c. (Time is in *hhmm* format.)

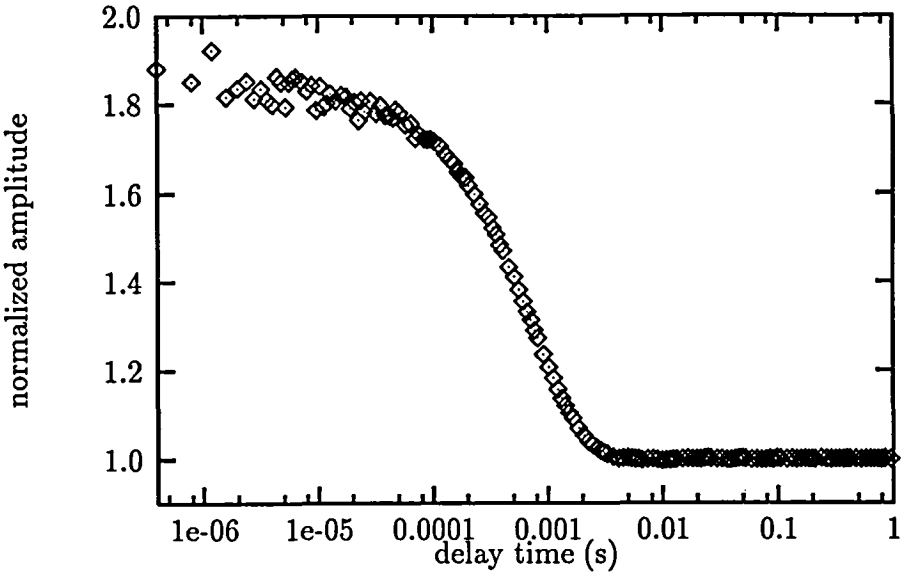

FIG. 6 A forward-scattering correlogram example showing simple exponential decay on a logarithmic time-scale. Taken at $T - T_c = 100$ mK at a laser power of 17 μW.

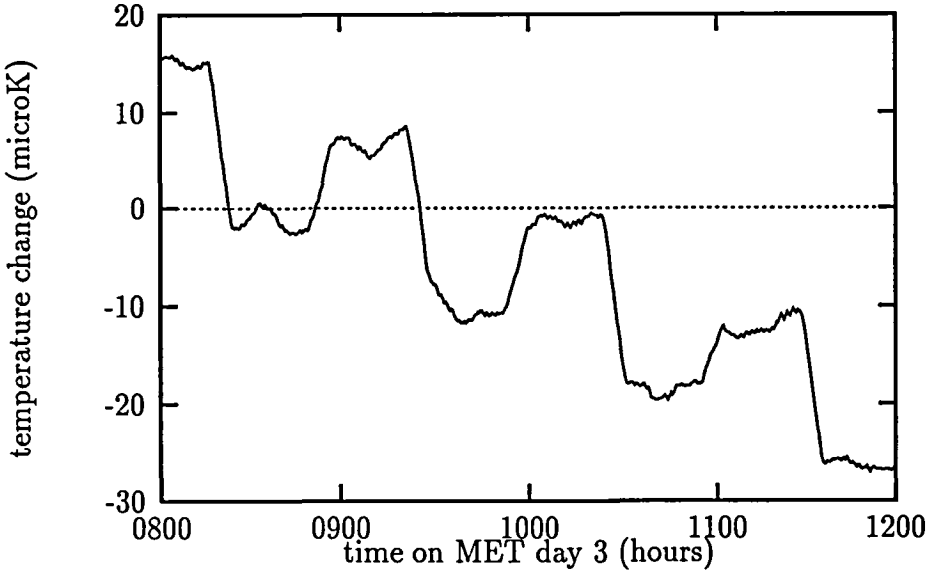

FIG. 7 A section of the zig-zag T_c search, showing the pattern of sample temperature changes: cooler by 20 μK, then warmer by 10 μK. The data are smoothed over a 300-second interval. The turbidity during this same time is shown in Fig. 8. (Time is in *hhmm* format.)

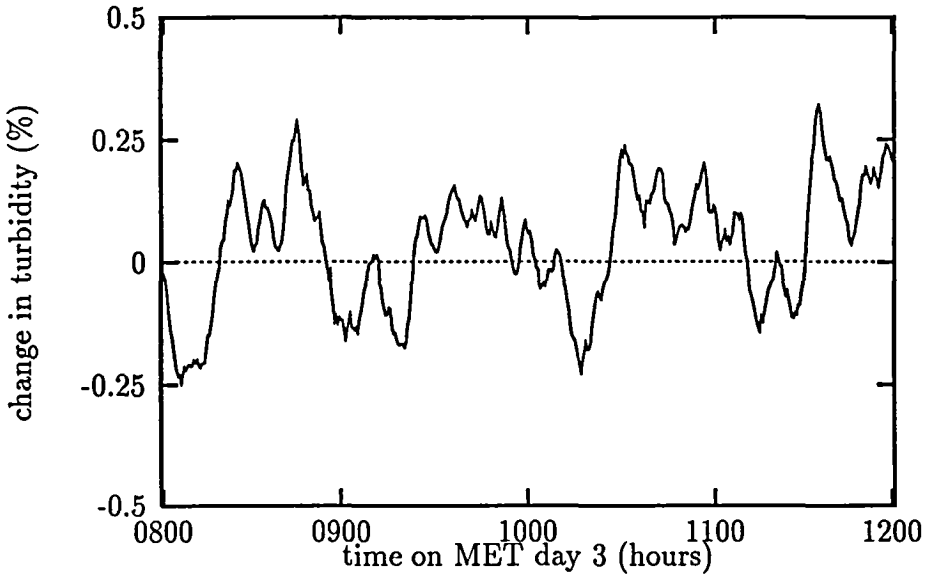

FIG. 8 A section of the zig-zag T_c search, showing the response of the sample turbidity to the zig-zag temperature steps shown in Fig. 7 for the same time period. The data are smoothed over a 300-second interval. (Time is in *hhmm* format.)

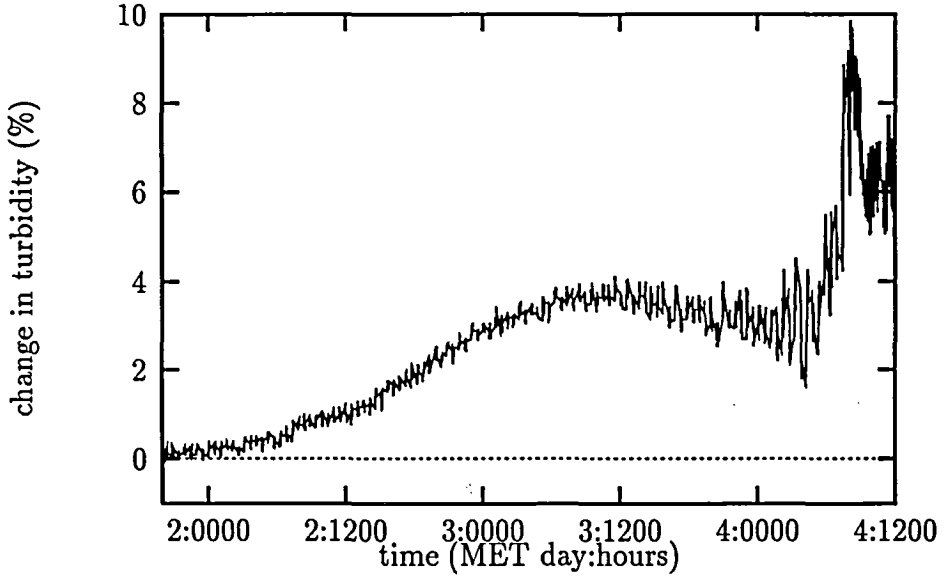

FIG. 9 The turbidity signal during the entire 64-hour zig-zag T_c search. (Time is in *day:hhmm* format.)

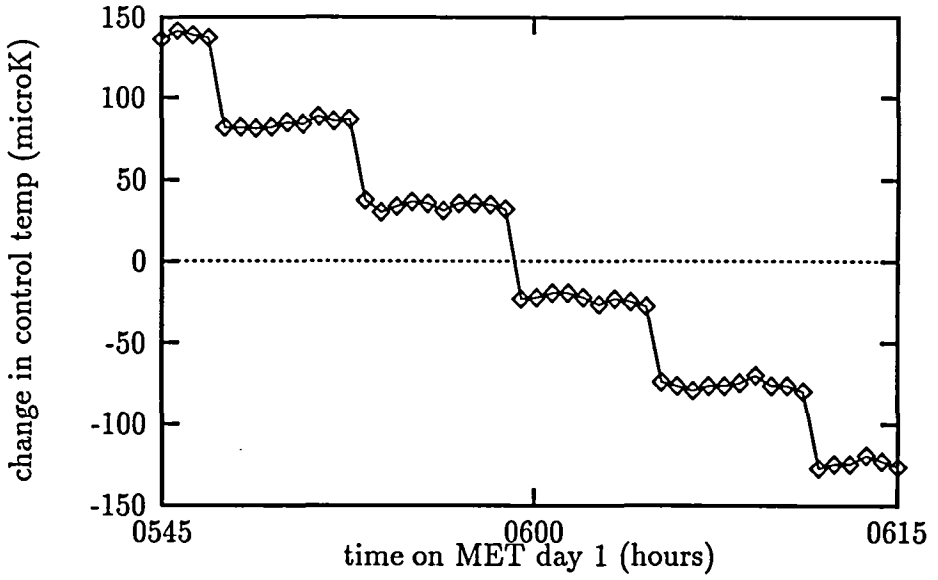

FIG. 10 The temperature of the high-precision control shell of the thermostat during the first scan for T_c. The temperature of this shell, shown making $-50\,\mu$K steps, determines the sample temperature, shown in Fig. 11. (Time is in *hhmm* format.)

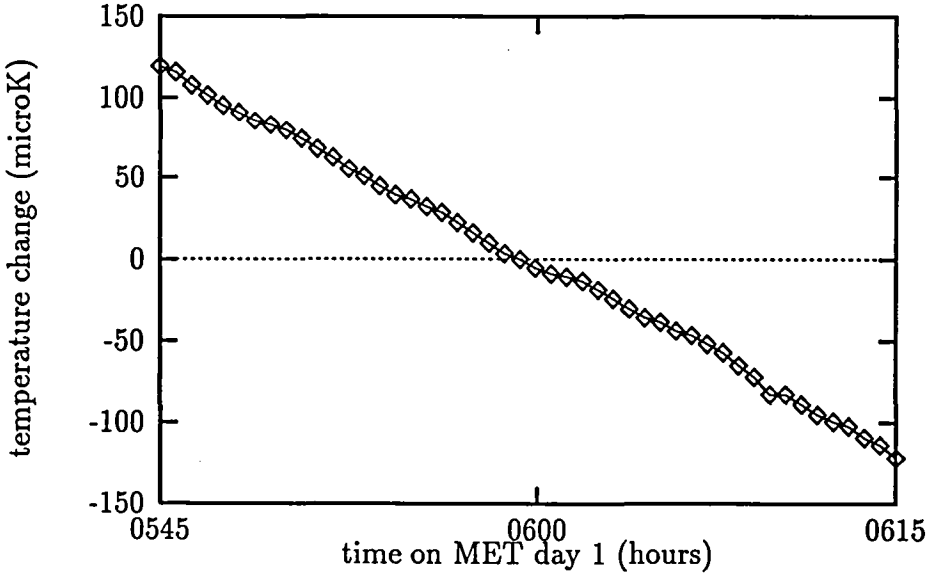

FIG. 11 The sample temperature during the first scan for T_c, in response to the control-shell steps shown in Fig. 10. The result is a uniform sample cooling of $500\,\mu$K/hour. (Time is in *hhmm* format.)

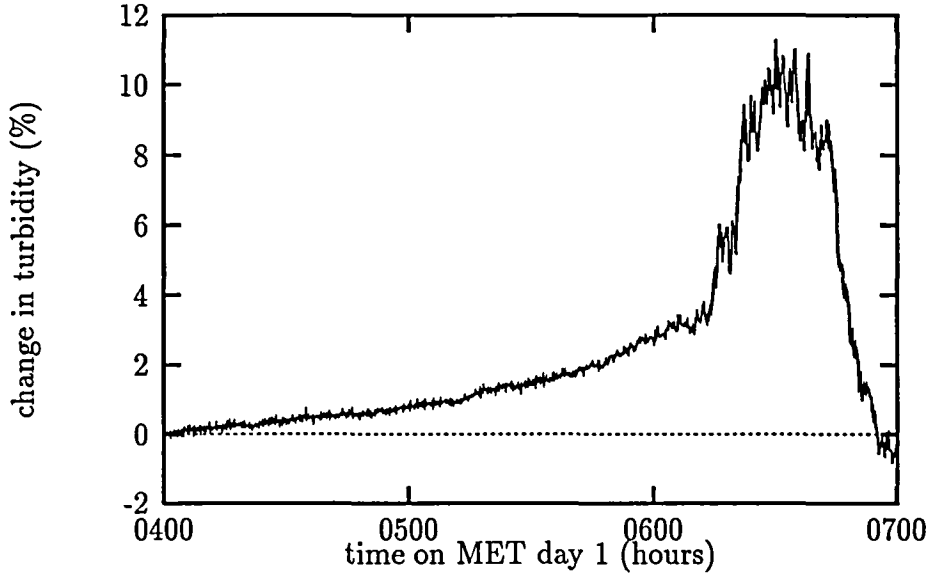

FIG. 12 The turbidity signal during the first scan for T_c. The small feature just past 0600 hours is where the sample crosses T_c; the large peak is spinodal decomposition. (Time is in *hhmm* format.)

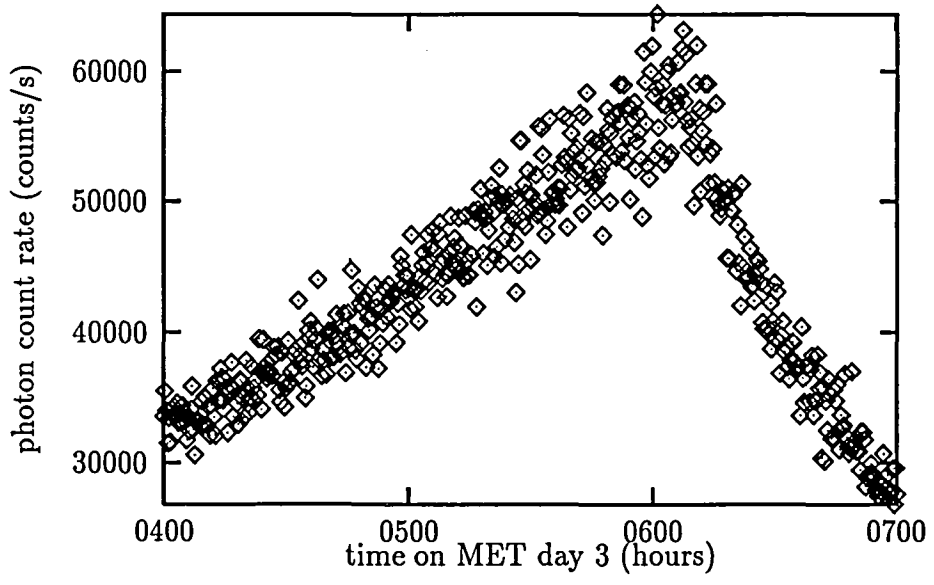

FIG. 13 Forward-scattering photon count rate during the first scan for T_c, showing from the break in slope that the sample crosses T_c just past 0600 hours. (Time is in *hhmm* format.)

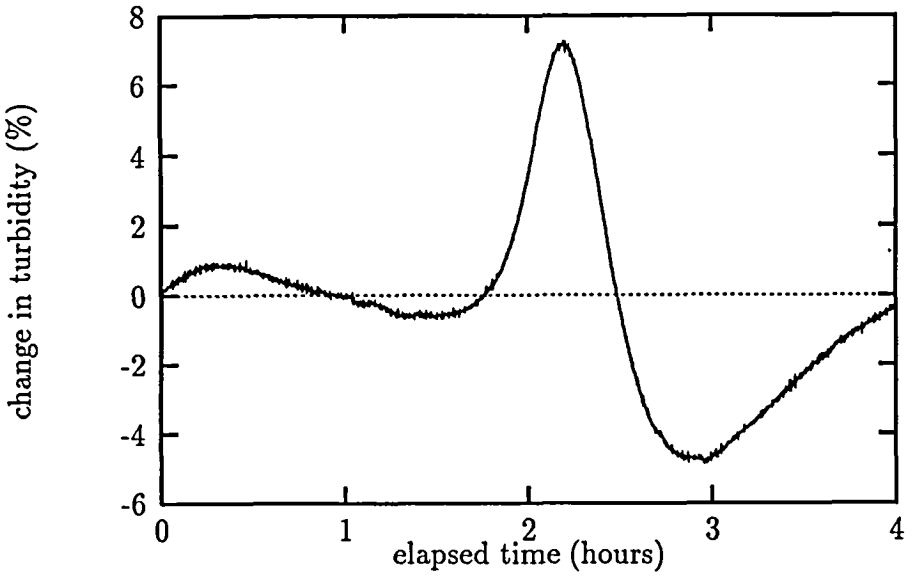

FIG. 14 The turbidity signal during a 500-μK/hour scan for T_c done in 1-g during preflight testing. Compare this scan with the μ-g scan shown in Fig. 12.

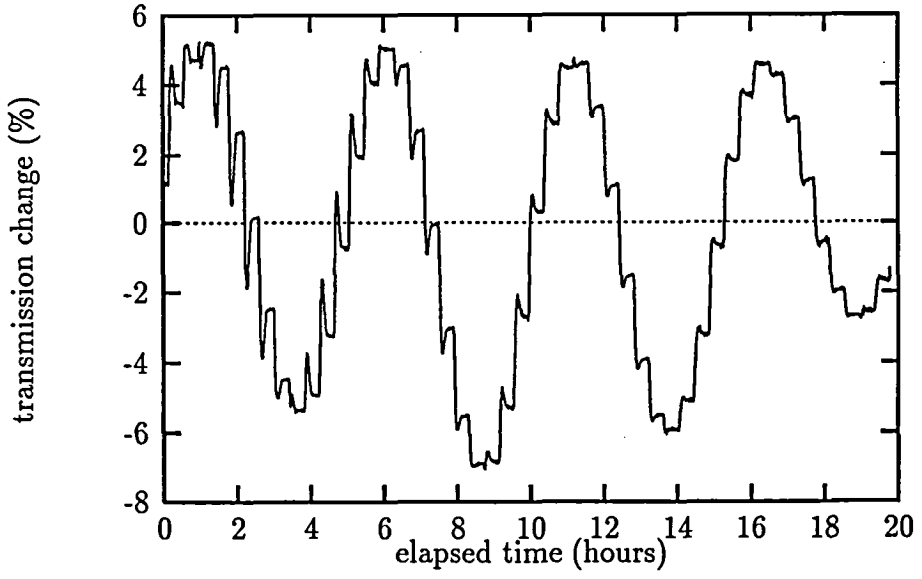

FIG. 15 The turbidity signal in preflight testing during a warming sequence between $T_c + 1$ K to $T_c + 5$ K, made in steps of 0.1 K. The sinusoidal shape is caused by cell expansion; the small spikes result from changes in fluid density.

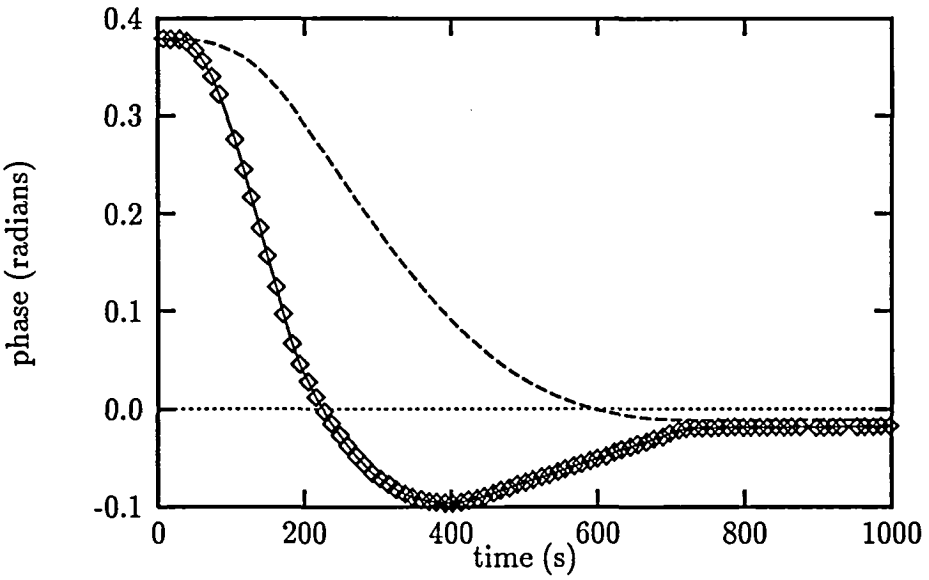

FIG. 16 Data taken on the engineering model of the instrument show, in the lower curve, the response of the turbidity signal to a change in temperature from $T_c + 0.6$ K to $T_c + 0.7$ K. The upper curve is the change solely caused by cell expansion. The vertical units are the phase along the interference curve for the cell.

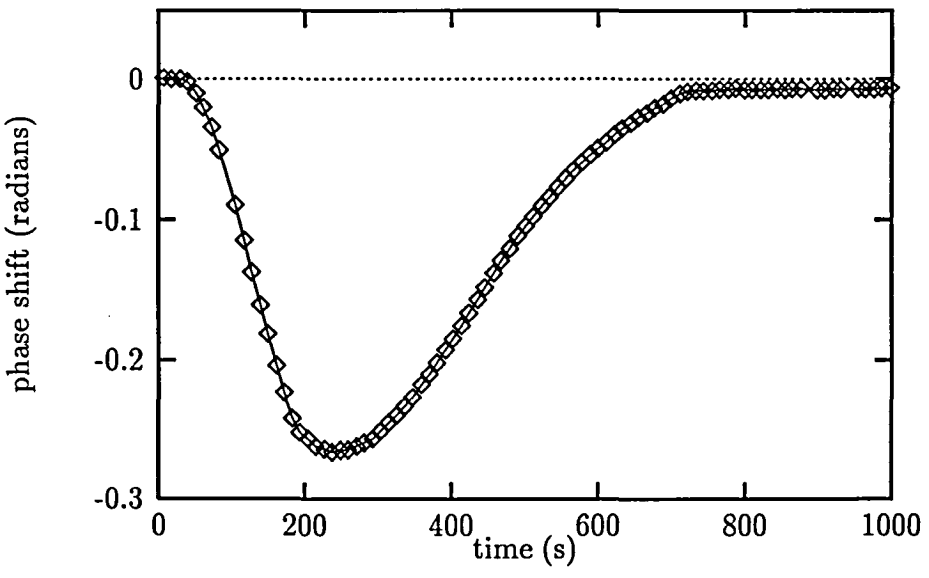

FIG. 17 The difference between the two curves in Fig. 16, showing the response of the turbidity signal solely caused by changes in the fluid density. Compare with Fig. 18. (These data are from the engineering model of the instrument).

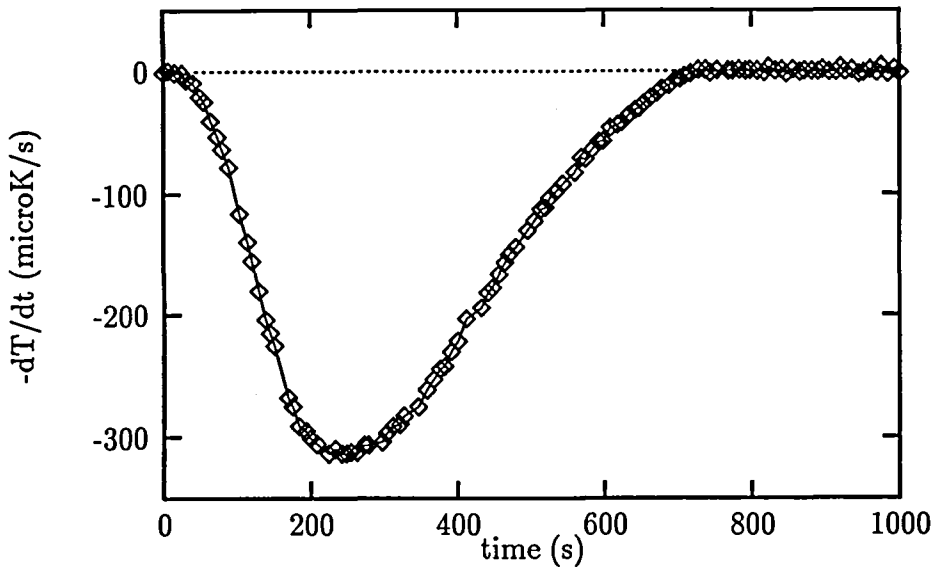

FIG. 18 The time derivative of the temperature change that produced the turbidity signal shown in Fig. 16. This curve has the same shape as the curve in Fig. 17. (These data are from the engineering model of the instrument).

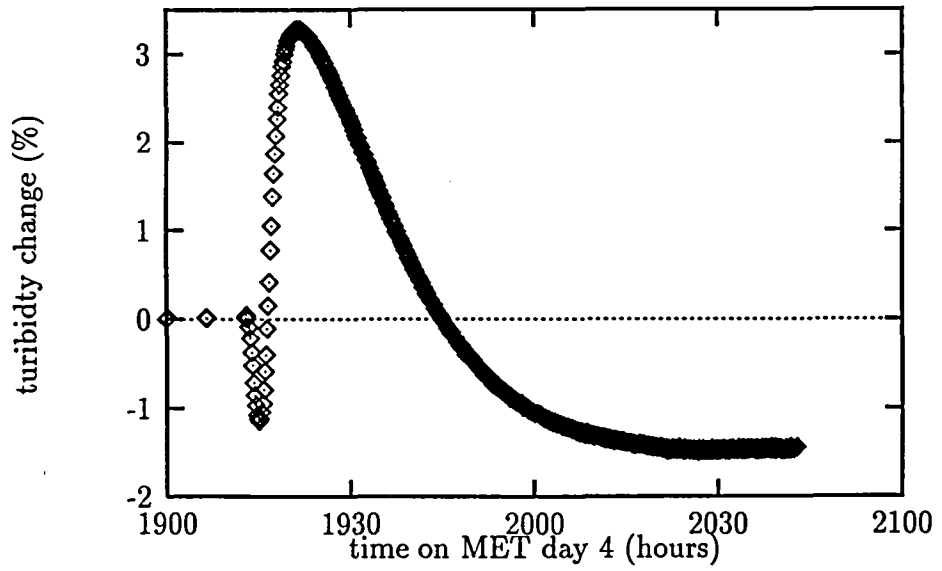

FIG. 19 The turbidity response to a temperature change of -70 mK starting at T_c+0.1 K, showing cell interference, adiabatic response, and an as-yet unidentified feature.

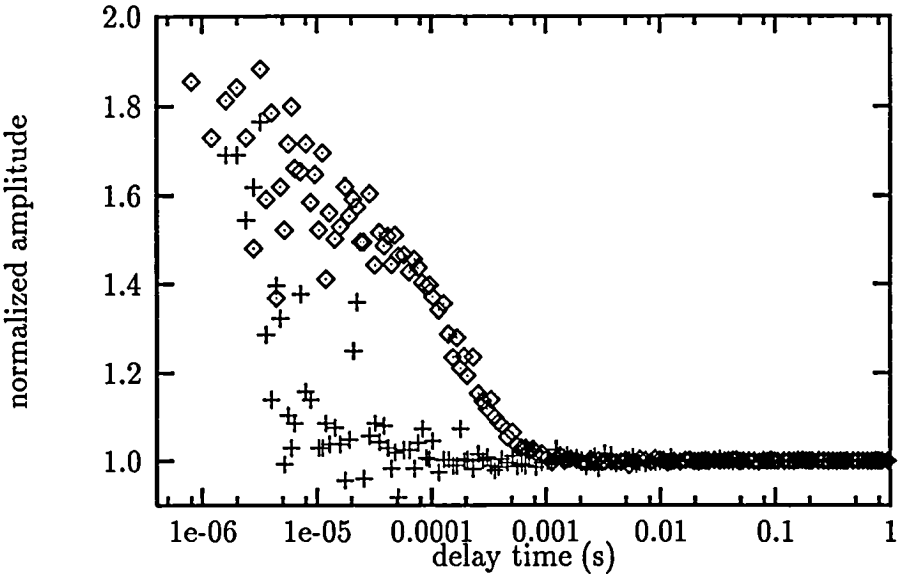

FIG. 20 Dual correlogram taken at $T_c + 560$ mK with 17 μW of laser power and 6-minute integration time. Average count rate for forward scattering (upper curve) was 710 counts/s; backscattering (lower curve), 435 counts/s.

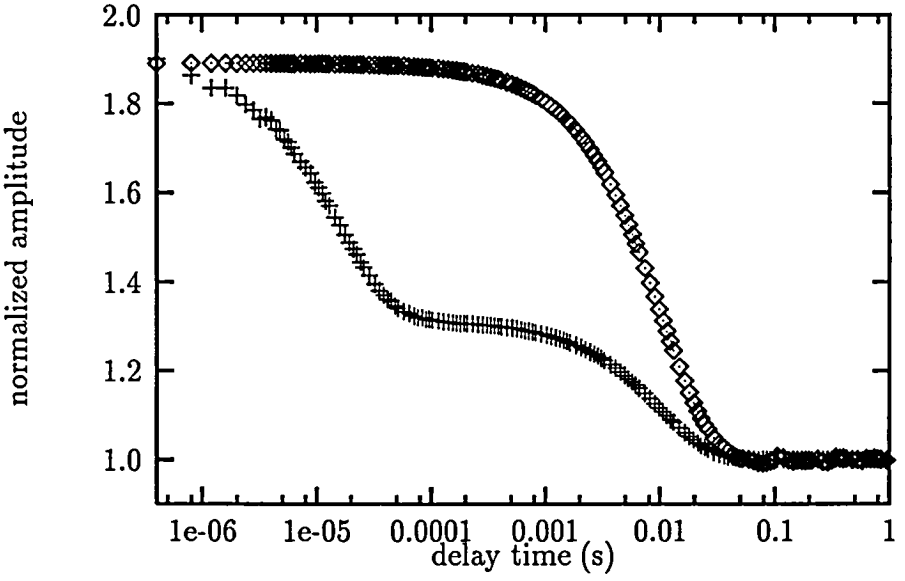

FIG. 21 Dual correlogram taken at $T_c + 1$ mK with 17 μW of laser power and 10-minute integration time. Average count rate for forward scattering (upper curve) was 446,000 counts/s; backscattering (lower curve), 17,800 counts/s.

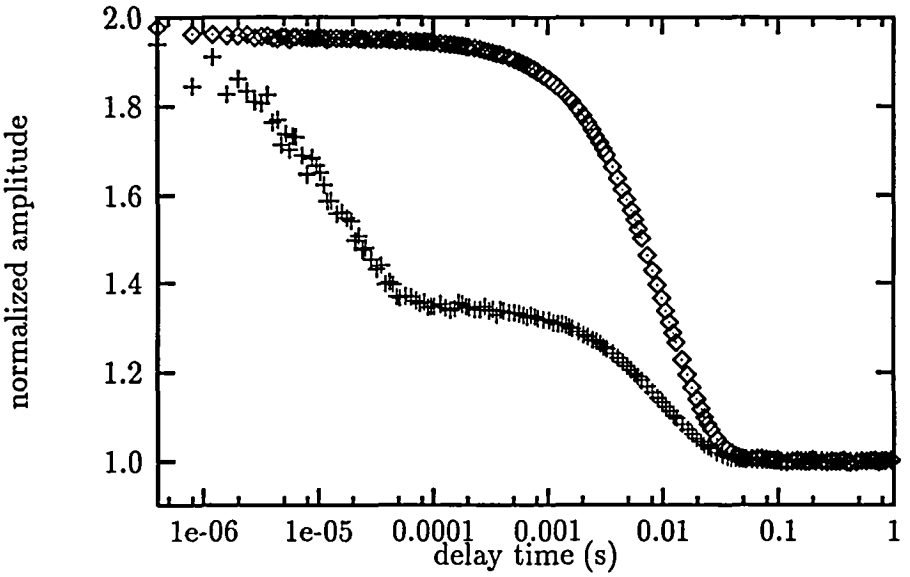

FIG. 22 Dual correlogram taken at $T_c + 1$ mK with 1.7 μW of laser power and 15-minute integration time. Average count rate for forward scattering (upper curve) was 27,100 counts/s; backscattering (lower curve), 2,200 counts/s.

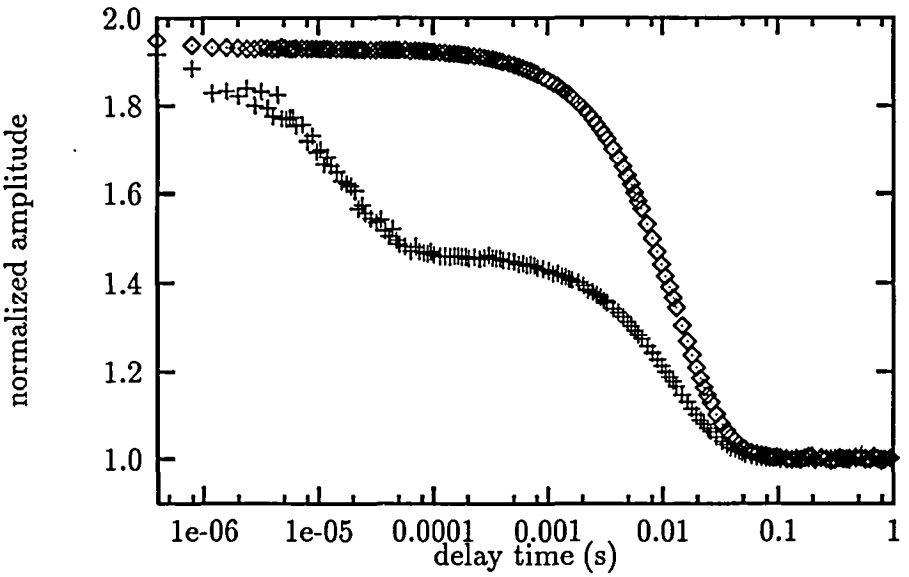

FIG. 23 Dual correlogram taken at $T_c + 100\,\mu$K with 1.7 μW of laser power and 15-minute integration time. Average count rate for forward scattering (upper curve) was 45,000 counts/s; backscattering (lower curve), 3,000 counts/s.

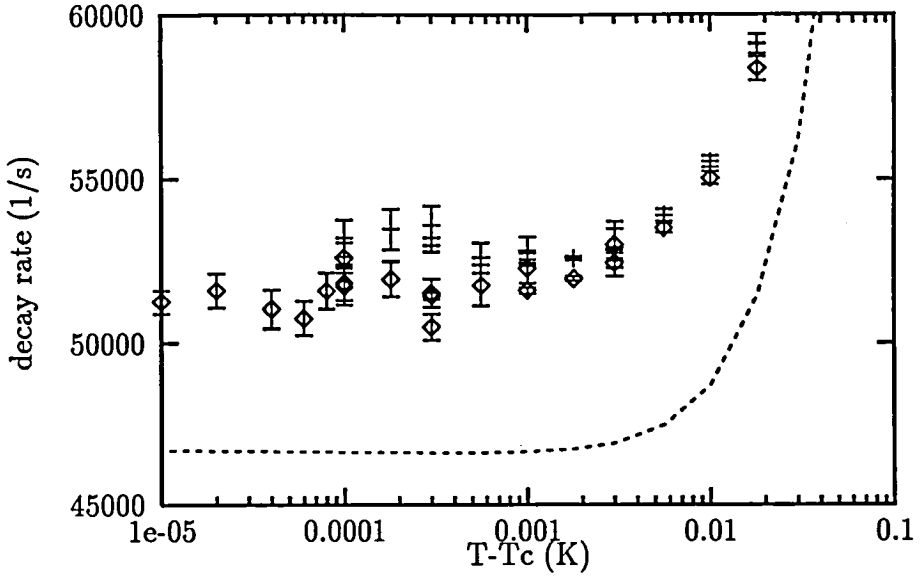

FIG. 24 Backscattering decay rates as a function of temperature. Vertical scale is linear and horizontal scale is logarithmic. Crosses are 1-g data from preflight testing diamonds are mission data. The curve is our best theoretical estimate and error bars show the rms of the data.

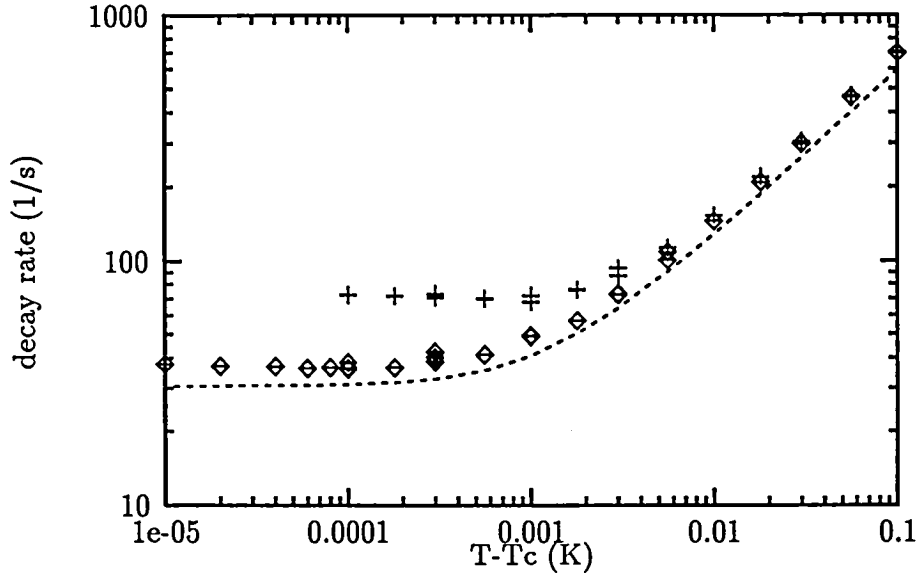

FIG. 25 Forward-scattering decay rates as a function of temperature. Both scales are logarithmic. Crosses are 1-g data from preflight testing; the diamonds are mission data. The curve is our best theoretical estimate and error bars, which are generally smaller than the symbols, show the rms of the data.

REPORT DOCUMENTATION PAGE

Form Approved
OMB No. 0704-0188

1. AGENCY USE ONLY (*Leave blank*)	2. REPORT DATE	3. REPORT TYPE AND DATES COVERED
	October 1995	Technical Memorandum

4. TITLE AND SUBTITLE
Highlights of the Zeno Results From the USMP-2 Mission

5. FUNDING NUMBERS
WU-963-50-00

6. AUTHOR(S)
Robert W. Gammon, J.N. Shaumeyer, Matthew E. Briggs, Hacène Boukari, David A. Gent, and R. Allen Wilkinson

7. PERFORMING ORGANIZATION NAME(S) AND ADDRESS(ES)
National Aeronautics and Space Administration
Lewis Research Center
Cleveland, Ohio 44135-3191

8. PERFORMING ORGANIZATION REPORT NUMBER
E-9848

9. SPONSORING/MONITORING AGENCY NAME(S) AND ADDRESS(ES)
National Aeronautics and Space Administration
Washington, D.C. 20546-0001

10. SPONSORING/MONITORING AGENCY REPORT NUMBER
NASA TM-107031

11. SUPPLEMENTARY NOTES
Robert W. Gammon, J.N. Shaumeyer, Matthew E. Briggs, Hacène Boukari, and David A. Gent, University of Maryland, College Park, Maryland 20742 (work funded by NASA Contract NAS3-25370); R. Allen Wilkinson, NASA Lewis Research Center. Responsible person, R. Allen Wilkinson, organization code 6712, (216) 433-2075.

12a. DISTRIBUTION/AVAILABILITY STATEMENT
Unclassified - Unlimited
Subject Category 77

This publication is available from the NASA Center for Aerospace Information, (301) 621-0390.

12b. DISTRIBUTION CODE

13. ABSTRACT (*Maximum 200 words*)

The Zeno instrument, a High-precision, light-scattering spectrometer, was built to measure the decay rates of density fluctuations in xenon near its liquid-vapor critical point in the low-gravity environment of the U.S. Space Shuttle. Eliminating the severe density gradients created in a critical fluid by Earth's gravity, we were able to make measurements to within 100 microKelvin of the critical point. The instrument flew for fourteen days in March, 1994 on the Space Shuttle Columbia, STS-62 flight, as part of the very successful USMP-2 payload. We describe the instrument and document its performance on orbit, showing that it comfortably reached the desired 3 microKelvin temperature control of the sample. Locating the critical temperature of the sample on orbit was a scientific challenge; we discuss the advantages and shortcomings of the two techniques we used. Finally we discuss problems encountered with making measurements of the turbidity of the sample, and close with the results of the measurement of the decay rates of the critical-point fluctuations.

14. SUBJECT TERMS	15. NUMBER OF PAGES
Critical point phenomena; Light scattering; Low-gravity research	29
	16. PRICE CODE: A03

17. SECURITY CLASSIFICATION OF REPORT	18. SECURITY CLASSIFICATION OF THIS PAGE	19. SECURITY CLASSIFICATION OF ABSTRACT	20. LIMITATION OF ABSTRACT
Unclassified	Unclassified	Unclassified	

National Aeronautics and
Space Administration

Lewis Research Center
21000 Brookpark Rd.
Cleveland, OH 44135-3191